Supporting Information for

Effect of Manganese Substitution of Ferrite Nanoparticles on Particle Grain Structure

Zichun Yan[1], Anish Chaluvadi[1,2], Sarah Spence[1], Christopher Bleyer[1], Jiazhou Zhu[2,†], Sara Fitzgerald[3], Thomas M. Crawford[3], Rachel B. Getman[2], John Watt[4], Dale L. Huber[5] and O. Thompson Mefford[1]

[1]Department of Materials Science & Engineering, Clemson University, Clemson, SC 29634, USA

[2]Department of Chemical & Biomolecular Engineering, Clemson University, Clemson, SC 29634, USA

[3]Department of Physics and Astronomy, SmartState Center for Experimental Nanoscale Physics, University of South Carolina, Columbia, South Carolina 29208, USA

[4]Center for Integrated Nanotechnologies, Los Alamos National Laboratory, Los Alamos, New Mexico, 87545, USA

[5]Center for Integrated Nanotechnologies, Sandia National Laboratories, Albuquerque, New Mexico 87185, USA

[†]Present address: CDU CN Novartis, Minhang District, Shanghai, China

Section S1. Ferrite Model Setup

Density functional theory (DFT) calculations were utilized to model different arrangements of the Mn ions within the ferrite crystal structure at different compositions. The ferrite model employed herein is based on the calculated bulk unit cell of Fe_3O_4. To create models with reasonably diverse arrangements, the base ferrite model was created with 8 Fe_3O_4 formula units, giving a base stoichiometry of $Fe_{24}O_{32}$. The unit cell is shown in Figure S1, and the atomic coordinates are given in Section S6. A total of up to 8 ion substitutions were carried out over 8 tetrahedral or 8 octahedral sites, for the normal or inverse spinel structure respectively, in the same unit cell resulting in a variety of ion arrangements. The 8 sites where substitutions were made are shown in Figure S1. Looking to compare with experimental results, five compositions of manganese substituted ferrites were tested: $Mn_0Fe_3O_4$, $Mn_{0.25}Fe_{2.75}O_4$, $Mn_{0.5}Fe_{2.5}O_4$, $Mn_{0.75}Fe_{2.25}O_4$, $Mn_1Fe_2O_4$. Ion arrangements considered for these different compositions are tabulated in Table S1. For each arrangement, we considered both normal and inverse spinel structures, yielding a total of 256 structures. The final reported saturation magnetization reported

for each of these compositions was based on the material with the lowest calculated electronic energy.

Table S1. Substitution of Mn2+ ion into ferrite site positions, where x's indicate sites where Mn was substituted for Fe.

	Site Positions								
	1	2	3	4	5	6	7	8	Identifier
Fe_3O_4									Fe3O4
$Mn_{0.25}Fe_{2.75}O_4$	x	x							Mn.25-1[b]
	x		x						Mn.25-2
	x			x					Mn.25-3[b]
	x				x				Mn.25-4
	x					x			Mn.25-5
	x						x		Mn.25-6[b]
	x							x	Mn.25-7
		x	x						Mn.25-8[b]
		x		x					Mn.25-9
		x			x				Mn.25-10
		x				x			Mn.25-11
		x					x		Mn.25-12
		x						x	Mn.25-13
			x	x					Mn.25-14
			x		x				Mn.25-15
			x			x			Mn.25-16
			x				x		Mn.25-17
			x					x	Mn.25-18
				x	x				Mn.25-19
				x		x			Mn.25-20
				x			x		Mn.25-

									21
				x				x	Mn.25-22
					x	x			Mn.25-23
					x		x		Mn.25-24
					x			x	Mn.25-25
						x	x		Mn.25-26
						x		x	Mn.25-27[b]
							x	x	Mn.25-28
$Mn_{0.5}Fe_{2.5}O_4$	x	x	x	x					Mn.5-1
	x	x	x		x				Mn.5-2
	x	x	x			x			Mn.5-3
	x	x	x				x		Mn.5-4
	x	x	x					x	Mn.5-5
	x	x		x	x				Mn.5-6
	x	x		x		x			Mn.5-7
	x	x		x			x		Mn.5-8
	x	x		x				x	Mn.5-9
	x	x			x	x			Mn.5-10
	x	x			x		x		Mn.5-11
	x	x			x			x	Mn.5-12
	x	x				x	x		Mn.5-13
	x	x				x		x	Mn.5-14
	x	x					x	x	Mn.5-15
	x		x	x	x				Mn.5-16
	x		x	x		x			Mn.5-17
	x		x	x			x		Mn.5-18
	x		x	x				x	Mn.5-19
	x		x		x	x			Mn.5-20
	x		x		x		x		Mn.5-21[a,b]
	x		x		x			x	Mn.5-22[a]
	x		x			x	x		Mn.5-23
	x		x			x		x	Mn.5-24[a]
	x		x				x	x	Mn.5-25
	x			x	x	x			Mn.5-26

	x			x	x		x		Mn.5-27
	x			x	x			x	Mn.5-28
	x			x		x	x		Mn.5-29
	x			x		x		x	Mn.5-30[a]
	x			x			x	x	Mn.5-31
	x				x	x	x		Mn.5-32
	x				x	x		x	Mn.5-33
	x				x		x	x	Mn.5-34
	x					x	x	x	Mn.5-35
		x	x	x	x				Mn.5-36
		x	x	x		x			Mn.5-37[b]
		x	x	x			x		Mn.5-38
		x	x	x				x	Mn.5-39
		x	x		x	x			Mn.5-40
		x	x		x		x		Mn.5-41
		x	x		x			x	Mn.5-42
		x	x			x	x		Mn.5-43
		x	x			x		x	Mn.5-44
		x	x				x	x	Mn.5-45
		x		x	x	x			Mn.5-46
		x		x	x		x		Mn.5-47
		x		x	x			x	Mn.5-48
		x		x		x	x		Mn.5-49
		x		x		x		x	Mn.5-50[b]
		x		x			x	x	Mn.5-51
		x			x	x	x		Mn.5-52
		x			x	x		x	Mn.5-53
		x			x		x	x	Mn.5-54
		x				x	x	x	Mn.5-55
			x	x	x	x			Mn.5-56
			x	x	x		x		Mn.5-57[b]
			x	x	x			x	Mn.5-58
			x	x		x	x		Mn.5-59
			x	x		x		x	Mn.5-60
			x	x			x	x	Mn.5-61
			x		x	x	x		Mn.5-62
			x		x	x		x	Mn.5-63
			x		x		x	x	Mn.5-64
			x			x	x	x	Mn.5-65
				x	x	x	x		Mn.5-66
				x	x	x		x	Mn.5-67

				x	x		x	x	Mn.5-68
				x		x	x	x	Mn.5-69
					x	x	x	x	Mn.5-70
$Mn_{0.75}Fe_{2.25}O_4$	x	x	x	x	x	x			Mn.75-1
	x	x	x	x	x		x		Mn.75-2
	x	x	x	x	x			x	Mn.75-3
	x	x	x	x		x	x		Mn.75-4
	x	x	x	x		x		x	Mn.75-5
	x	x	x	x			x	x	Mn.75-6
	x	x	x		x	x	x		Mn.75-7
	x	x	x		x	x		x	Mn.75-8
	x	x	x		x		x	x	Mn.75-9
	x	x	x			x	x	x	Mn.75-10
	x	x		x	x	x	x		Mn.75-11
	x	x		x	x	x		x	Mn.75-12
	x	x		x	x		x	x	Mn.75-13
	x	x		x		x	x	x	Mn.75-14
	x	x			x	x	x	x	Mn.75-15
	x		x	x	x	x	x		Mn.75-16
	x		x	x	x	x		x	Mn.75-17
	x		x	x	x		x	x	Mn.75-18
	x		x	x		x	x	x	Mn.75-19
	x		x		x	x	x	x	Mn.75-20
	x			x	x	x	x	x	Mn.75-21
		x	x	x	x	x	x		Mn.75-22
		x	x	x	x	x		x	Mn.75-23
		x	x	x	x		x	x	Mn.75-24
		x	x	x		x	x	x	Mn.75-25[b]

		x	x		x	x	x	x	Mn.75-26
		x		x	x	x	x	x	Mn.75-27
			x	x	x	x	x	x	Mn.75-28
$MnFe_2O_4$	x	x	x	x	x	x	x	x	MnFe2O4

[a] Inverse spinel electronic structure did not converge.
[b] Normal spinel electronic structure did not converge.

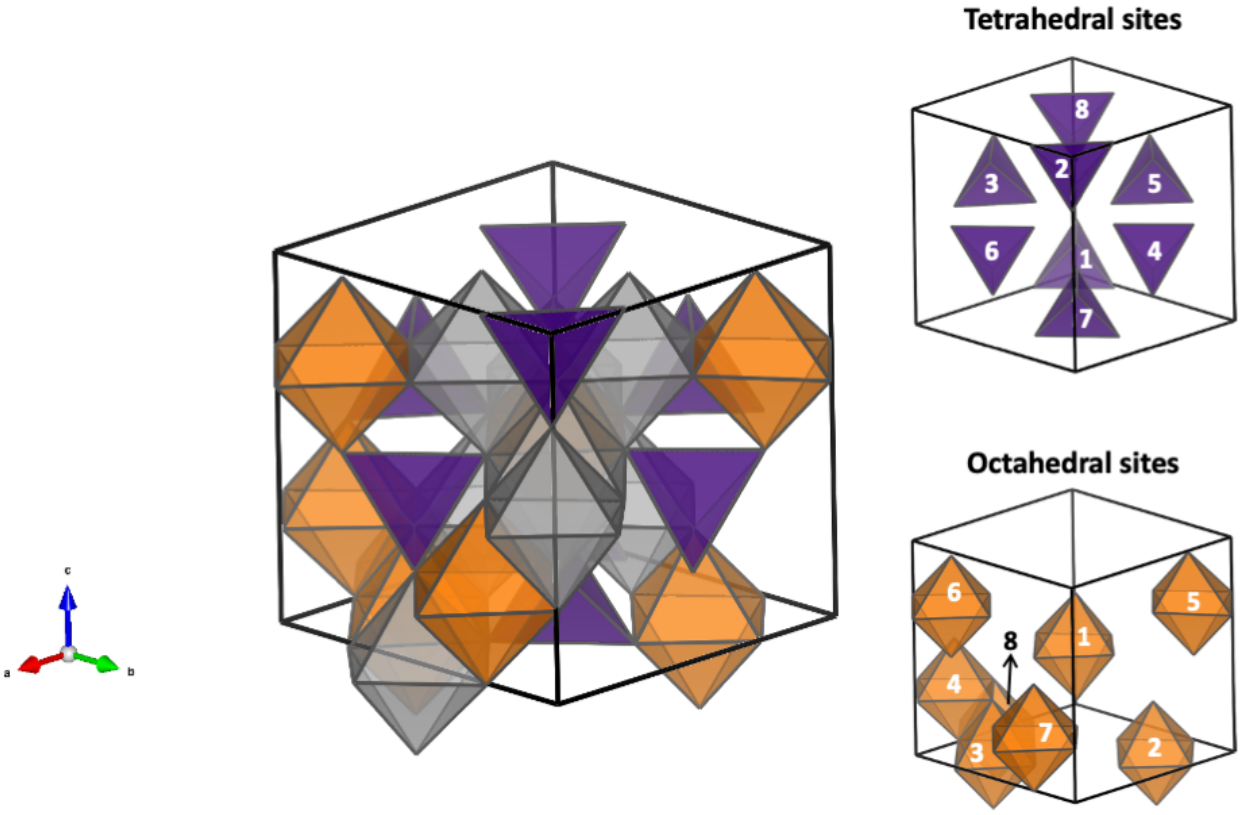

Figure S1. Polyhedral representation of the unit cell employed in this work with tetrahedral sites labeled in purple and octahedral sites labeled in orange and gray. Substitutions were made into the tetrahedral sites, or the octahedral sites colored in orange.

Section S2. Additional Computational Parameters for DFT Calculations

Additional details about the DFT calculations that were not discussed in the main text are discussed below. Additionally, sample input files are provided in **Section S6**.

The substituent atom, Mn^{2+}, is a divalent cation which can exist in high-spin or low-spin states. Initial guesses for the spin state are controlled using the MAGMOM flag in the INCAR file (see Section S6). Test calculations performed on a subset of structures indicate that the electronic structure converges to the high spin state regardless of whether the initial guess for the DFT calculations is high spin or low spin.

The DFT+U formalism was utilized to capture the strong Coulombic repulsion for 3d electrons on the Mn and Fe atoms and to further prevent the delocalization of electrons in these semiconducting materials. The DFT calculations employed herein employed U_{eff}, which was computed as the subtraction U−J, where U and J values for each ion type were taken from the Materials Project Database.[1] U and J values for each ion type used can be found below in Table S2. More information is provided in Section S6.

Table S2. U and J parameters used for metal ions in DFT calculations

Metal	**U value (eV)**	**J value (eV)**
Mn	3.90	0.00
Fe	5.30	0.00

Unit cell optimizations consisted of two steps (referred to below as the "two-step" method). First, unit cell relaxations were made to allow cell volume, cell shape, and ionic position changes (ISIF = 3 in the VASP INCAR; see Section S6). Once converged, geometric relaxations were performed restricting the cell volume and cell shape but allowing the ionic positions to change (convert CONTCAR to POSCAR and set ISIF = 2 in the VASP INCAR; see Section S6). This strategy was employed for every composition and configuration. Relaxation using this method

resulted in slightly non-cubic unit cells, for example, with unit cell angles of $\alpha = 90.194°$, $\beta = 89.943°$, $\gamma = 90.002°$.

Section S3. Validation of Unit Cell Volume and Influence on Unit Cell Magnetic Moment.

Unit cell volume obtained using the two-step method elaborated above was compared with another strategy where the lattice parameter was varied while keeping the unit cell shape fixed (in a cube). This method is referred to below as the "manual" method. This method was employed for a small subset of structures. In these calculations, the ion positions were allowed to relax at each value of the lattice parameter. For example, energies versus lattice parameter are shown for the most energetically favorable state of $MnFe_2O_4$ in Figure S2. Using this method, the optimal lattice parameter of $MnFe_2O_4$ is 8.55 Å. In comparison, the lattice parameter using the two-step method is 8.59 Å. The experimentally observed lattice parameter for $MnFe_2O_4$ is 8.511 Å.[2] Further comparisons between this manual lattice parameter convergence strategy and the two-step method described above are provided in Table S3. In all calculations tested, the method for obtaining the unit cell volume had no influence on the calculated unit cell magnetic moment (however the minor differences in cell volume propagated into the computed saturation magnetizations).

Figure S2. Unit cell optimization of $MnFe_2O_4$ using the manual method.

Table S3. Comparison between lattice parameters derived from manual optimization strategy and two-step optimization strategy. All values are in Å.

Ferrite	Manual Optimization Strategy	Two-Step Optimization Strategy
MnFe2O4	8.55	8.59
Mn0.375Fe2.625O4	8.55	8.55
Mn0.375Co0.25Fe2.375O4	8.55	8.51
Mn0.25Co0.375Fe2.375O4	8.53	8.49

Section S4. Normal versus Inverse Spinel.

Bulk ferrite structures (i.e., either normal or inverse spinel) and their corresponding saturation magnetizations were reported for the lowest energy structure at each composition according to DFT. For Fe_3O_4 we tried initial guesses for both the inverse and normal spinel

structure, but they both converged to the inverse spinel structure, indicating that Fe_3O_4 prefers the inverse spinel structure as expected. We find that all compositions comprising Mn prefer the normal spinel structure (Figure S3) and that this preference for the normal spinel structure increases with increasing manganese composition.

$MnFe_2O_4$ is a unique ferrite in that because Mn^{2+} and Fe^{3+} have the same number of unpaired electrons, both inverse and normal spinel states of $MnFe_2O_4$ result in the same Ms. Therefore, starting with an inverse Fe_3O_4, increasing Mn content should increase Ms, which is indeed what we find in our calculations. Starting with a normal Fe_3O_4 (unnatural) spinel, increasing Mn content should decrease Ms, due to the negative exchange coupling between A and B sites. However, we find that in our normal spinel structures, some of the Fe^{3+} in the B sites convert to Fe^{2+} upon incorporation of Mn (into the A sites). Specifically, there are 6, 4, 2, and 0 Fe^{2+} occupying B sites in the $Mn_{0.25}Fe_{2.75}O_4$, $Mn_{0.5}Fe_{2.5}O_4$, $Mn_{0.75}Fe_{2.25}O_4$, and $Mn_1Fe_2O_4$ structures, respectively. This can be somewhat rationalized by conferring with the experimental trend that Mn substitutes into tetrahedral sites preferentially: $MnFe_2O_4$ is a notoriously well-known mixed spinel where ~80% substitutes to A sites and ~20% substitutes to B sites. The result is that, for every composition, the unit cell magnetic moment is the same, regardless of the arrangement of Mn ions and regardless of whether the crystal structure is normal or inverse spinel. Unit cell magnetic moments and saturation magnetizations for the lowest energy structures at each composition are provided in Table S4.

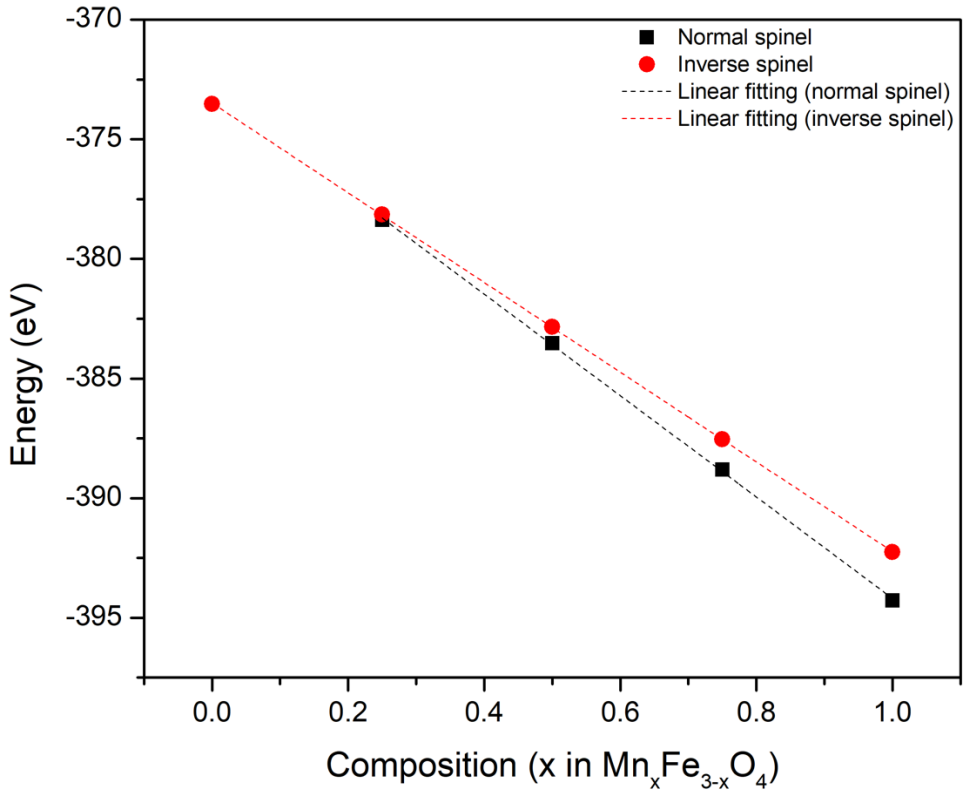

Figure S3. Lowest energies for inverse or normal spinel structure at each composition.

Table S4. Magnetic moment and saturation magnetization of lowest energy structure at different levels of Mn substitution.

x in $Mn_xFe_{3-x}O_4$	Unit cell magnetic moment (Bohr magnetons per formula unit)	Saturation magnetization (emu/g, Am^2/kg)
0	4	96.5
0.25	4.25	102.6
0.5	4.5	108.8
0.75	4.75	114.9
1	5	121.1

Section S5. Unit Conversions.

To convert from the magnetic moment in Bohr magnetons to saturation magnetization in emu/g, Equation S1 was used seen below, where μB represents Bohr magneton and Wb*m stands for Weber-meters. The magnetic moment was divided by the density, which was computed for each structure based on the molar weights and the calculated unit cell volumes.

$$\left[\frac{emu}{g}\right] = \frac{1\ [\mu B] * \frac{(1.1653 * 10^{-29})[Wb * m]}{[\mu B]} * \frac{(7.96 * 10^{8})[emu]}{[Wb * m]}}{[\frac{g}{cm^3}]}$$

Equation S1.

Section S6. Example Input Files

POSCAR: This is the base file. Substitutions are made by replacing Fe for Mn in sites 1-8. See Table S1 for more details.

```
Fe3 O4
   8.55000000000000
     1.0000000000000000    0.0000000000000000    0.0000000000000000
     0.0000000000000000    1.0000000000000000    0.0000000000000000
     0.0000000000000000    0.0000000000000000    1.0000000000000000
   Fe   O
    24    32
Direct
  0.1250000000000000  0.1250000000000000  0.1250000000000000 #site 1 tetrahedral
  0.8750000000000000  0.8750000000000000  0.8750000000000000 #site 2 tetrahedral
  0.6250000000000000  0.1250000000000000  0.6250000000000000 #site 3 tetrahedral
  0.3750000000000000  0.8750000000000000  0.3750000000000000 #site 4 tetrahedral
  0.1250000000000000  0.6250000000000000  0.6250000000000000 #site 5 tetrahedral
  0.8750000000000000  0.3750000000000000  0.3750000000000000 #site 6 tetrahedral
  0.6250000000000000  0.6250000000000000  0.1250000000000000 #site 7 tetrahedral
  0.3750000000000000  0.3750000000000000  0.8750000000000000 #site 8 tetrahedral
  0.5000000000000000  0.5000000000000000  0.5000000000000000
  0.2500000000000000  0.7500000000000000  0.0000000000000000
  0.7500000000000000  0.2500000000000000  0.0000000000000000
  0.7500000000000000  1.0000000000000000  0.5000000000000000
  0.2500000000000000  0.0000000000000000  0.7500000000000000
  0.0000000000000000  0.2500000000000000  0.7500000000000000
  1.0000000000000000  0.7500000000000000  0.2500000000000000
  0.5000000000000000  0.0000000000000000  0.0000000000000000
  0.2500000000000000  0.2500000000000000  0.5000000000000000 #site 1 octahedral
```

0.7500000000000000 0.7500000000000000 0.5000000000000000 #site 2 octahedral
0.7500000000000000 0.5000000000000000 0.7500000000000000 #site 3 octahedral
0.2500000000000000 0.5000000000000000 0.2500000000000000 #site 4 octahedral
1.0000000000000000 0.5000000000000000 0.0000000000000000 #site 5 octahedral
0.5000000000000000 0.2500000000000000 0.2500000000000000 #site 6 octahedral
0.5000000000000000 0.7500000000000000 0.7500000000000000 #site 7 octahedral
0.0000000000000000 1.0000000000000000 0.5000000000000000 #site 8 octahedral
0.2500000000000000 0.2500000000000000 0.2500000000000000
0.7500000000000000 0.7500000000000000 0.7500000000000000
0.5000000000000000 1.0000000000000000 0.7500000000000000
0.5000000000000000 0.0000000000000000 0.2500000000000000
0.0000000000000000 0.7500000000000000 0.5000000000000000
0.0000000000000000 0.2500000000000000 0.5000000000000000
0.7500000000000000 0.5000000000000000 0.0000000000000000
0.2500000000000000 0.5000000000000000 0.0000000000000000
0.0000000000000000 0.5000000000000000 0.2500000000000000
0.0000000000000000 0.5000000000000000 0.7500000000000000
0.5000000000000000 0.2500000000000000 1.0000000000000000
0.5000000000000000 0.7500000000000000 1.0000000000000000
0.2500000000000000 1.0000000000000000 0.5000000000000000
0.7500000000000000 0.0000000000000000 0.5000000000000000
0.2500000000000000 0.7500000000000000 0.7500000000000000
0.7500000000000000 0.2500000000000000 0.2500000000000000
0.5000000000000000 0.5000000000000000 0.2500000000000000
0.5000000000000000 0.5000000000000000 0.7500000000000000
1.0000000000000000 0.2500000000000000 1.0000000000000000
0.0000000000000000 0.7500000000000000 1.0000000000000000
1.0000000000000000 0.0000000000000000 0.7500000000000000
1.0000000000000000 0.0000000000000000 0.2500000000000000
0.5000000000000000 0.7500000000000000 0.5000000000000000
0.5000000000000000 0.2500000000000000 0.5000000000000000
0.7500000000000000 0.2500000000000000 0.7500000000000000
0.2500000000000000 0.7500000000000000 0.2500000000000000
0.2500000000000000 0.5000000000000000 0.5000000000000000
0.7500000000000000 0.5000000000000000 0.5000000000000000
0.7500000000000000 0.0000000000000000 0.0000000000000000
0.2500000000000000 1.0000000000000000 0.0000000000000000
0.7500000000000000 0.7500000000000000 0.2500000000000000
0.2500000000000000 0.2500000000000000 0.7500000000000000

INCAR:

ALGO = Fast
EDIFF = 1E-5
ENCUT = 520
IBRION = 2

ICHARG = 1
ISIF = 3 #ISIF = 2 if on second step of unit cell optimization
ISMEAR = -5
ISPIN = 2
LDAU = True
LDAUJ = 0 0
LDAUL = 2 0 # equals 2 for Fe and Mn and 0 for O
LDAUPRINT = 1
LDAUTYPE = 2
LDAUU = 5.3 0 # equals 5.3 for Fe, 3.9 for Mn, and 0 for O
LORBIT = 11
LREAL = Auto
LWAVE = False
MAGMOM = 8*5.0 8*-5.0 8*-4.0 32*0.6 # initial guesses are explained below
NELM = 500
NSW = 99
PREC = Accurate
SIGMA = 0.05

LMAXMIX = 6
AMIX = 0.1
AMIX_MAG = 0.2
BMIX = 0.0001
BMIX_MAG = 0.0001

Initial guesses for MAGMOM flag:

- For Fe in tetrahedral sites: 5.0
- For Fe in octahedral sites 1-8: -4.0
- For Fe in remaining octahedral sites: -5.0
- For Mn in tetrahedral sites: 5.0
- For Mn in octahedral sites 1-8: -5.0

POTCARs used in this work:

Results from executing grep PBE POTCAR at the command prompt:

PAW_PBE Fe_pv 02Aug2007
TITEL = PAW_PBE Fe_pv 02Aug2007
PAW_PBE Mn_pv 02Aug2007
TITEL = PAW_PBE Mn_pv 02Aug2007
PAW_PBE O 08Apr2002
TITEL = PAW_PBE O 08Apr2002

KPOINTS:
k-points
0
gamma
5 5 5
0 0 0

Section S7. Langevin fitting using SPfit

The sample weight was measured and calculated via ICP-OES. The SPfit program calculates the

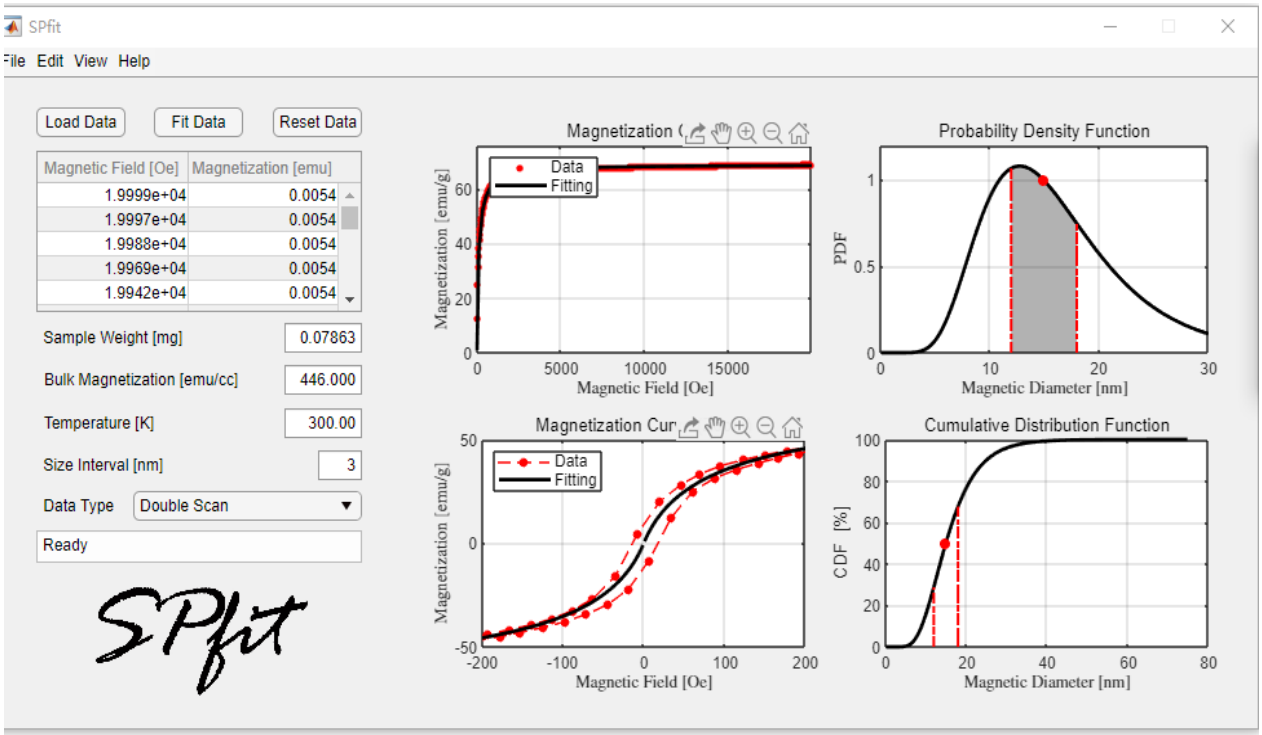

Figure S4 Program interface of SPfit of a successfully fitted sample.

probability density function and cumulative distribution function along with the fitted magnetization curves. The examples of successful fitting and unsuccessful fitting are shown in

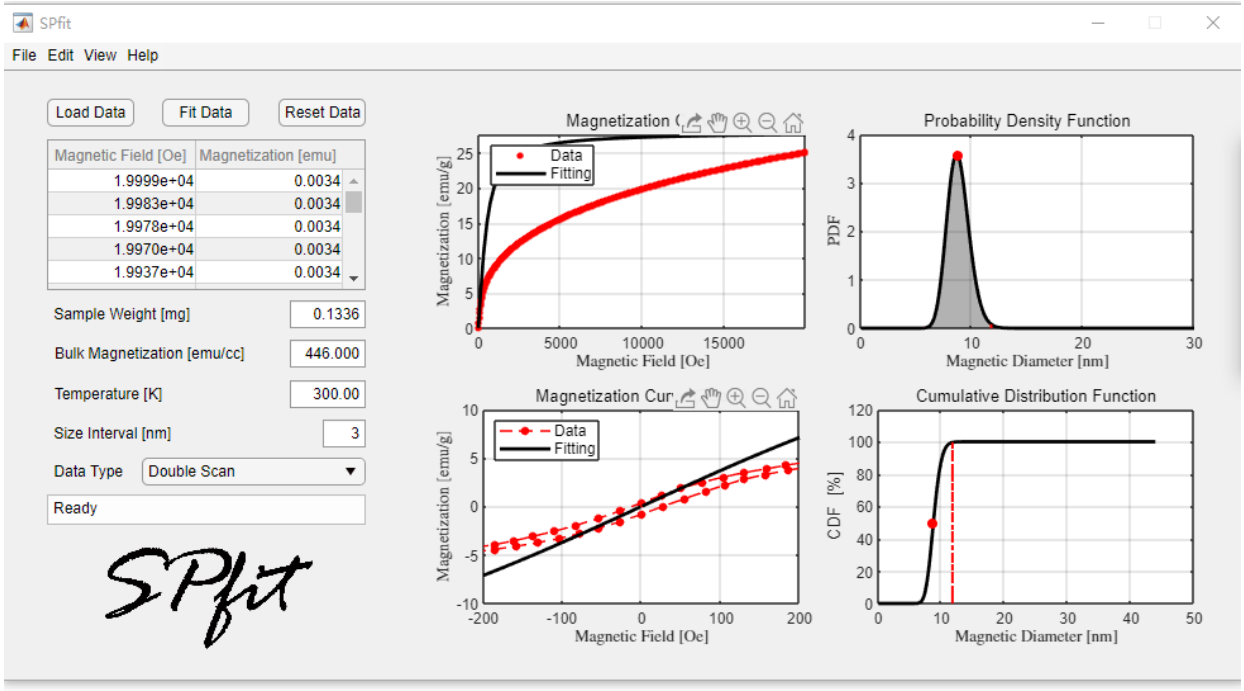

Figure S5 Program interface of SPfit of an unsuccessfully fitted sample.

Figure. S4 and Figure S5, respectively.

References

1. Jain, A.; Ong, S. P.; Hautier, G.; Chen, W.; Richards, W. D.; Dacek, S.; Cholia, S.; Gunter, D.; Skinner, D.; Ceder, G.; Persson, K. a. The Materials Project: A materials genome approach to accelerating materials innovation. APL Materials **2013**, 1, 011002.
2. Brik, M. G.; Suchocki, A.; Kamińska, A. Lattice Parameters and Stability of the Spinel Compounds in Relation to the Ionic Radii and Electronegativities of Constituting Chemical Elements. Inorganic Chemistry **2014** *53*(10), 5088-5099, DOI: 10.1021/ic500200a.